

NASA Technical Memorandum 104368
ICOMP-91-06; CMOTT-91-01

1N-34
13488
P.24

Low Reynolds Number Two-Equation Modeling of Turbulent Flows

V. Michelassi and T.-H. Shih
*Institute for Computational Mechanics in Propulsion
and Center for Modeling of Turbulence and Transition
Lewis Research Center
Cleveland, Ohio*

(NASA-TM-104368) LOW REYNOLDS NUMBER
TWO-EQUATION MODELING OF TURBULENT FLOWS
(NASA) 24 p CSCL 200

N91-23416

Unclas
0013488

G3/34

May 1991





Low Reynolds Number Two-Equation Modeling of Turbulent Flow

V. Michelassi* and T.-H. Shih

Institute for Computational Mechanics in Propulsion
and Center for Modeling of Turbulence and Transition
Lewis Research Center
Cleveland, Ohio 44135

Abstract

A new $k - \epsilon$ turbulence model that accounts for viscous and wall effects is presented. The proposed formulation does not contain the local wall distance thereby making very simple the application to complex geometries. The formulation is based on an existing $k - \epsilon$ model that proved to fit very well with the results of direct numerical simulation. The new form is compared with nine different two-equation models and with direct numerical simulation for a fully developed channel flow at $Re = 3300$. The simple flow configuration allows a comparison free from numerical inaccuracies. The computed results prove that few of the considered forms exhibit a satisfactory agreement with the channel flow data. The new model shows an improvement with respect to the existing formulations.

1 Introduction

The Reynolds averaging of the Navier-Stokes equations ($N - S$) allows solving very complex flow configurations with a manageable computer effort [1, 2]. A possible alternative approach is the so called *Direct Numerical Simulation*[3], (DNS), that, because of the current memory and speed limitations of supercomputers, is restricted to simple flows and low Reynolds numbers (Re). So, the solution of the Reynolds averaged $N - S$ equations still represents the main possibility for flow simulation in engineering applications. The well known drawback of the Reynolds averaging technique lies in the introduction of further unknowns, the so called *Reynolds Stresses*, stemming from averaging of the non-linear convective terms.

The Reynolds stress components are normally related to the mean flow quantities through a set of additional equations that represent the turbulence model. It is possible to carry out a further simplification following the Boussinesq assumption in

*on leave from the University of Florence, Italy

which the Reynolds stress components are expressed in terms of the mean velocity gradients as follows:

$$-\overline{u_i u_j} = \nu_t \left(\frac{\partial U_j}{\partial x_i} + \frac{\partial U_i}{\partial x_j} \right) - \frac{2}{3} k \delta_{ij} \quad (1)$$

in which $k = \frac{1}{2} \sum_{i=1}^3 \overline{u_i u_i}$ is the turbulent kinetic energy, u_i is the fluctuating velocity, U_i is the mean velocity, ν_t is the *turbulent viscosity* that represents the proportionality parameter between the Reynolds stress and the mean strain rate, and the overbar stands for the average operator. The turbulent viscosity ν_t is generally related to the local velocity and length scale of turbulence.

Accordingly, it is possible to define two main model categories, with decreasing complexity, that have an acceptable degree of generality:

- **Full Reynolds Stress models.** This approach does not use the Boussinesq assumption and every component of the Reynolds stress tensor is computed using a transport equation. Due to the high non-linearity usually connected to the source terms of the differential system, this class of models requires numerical methods which can effectively treat the stiffness introduced by the source terms.
- **Two-Equation models.** In these lower order models the Reynolds stress components are computed taking advantage of the Boussinesq assumption so that the degree of complexity of the formulation is considerably reduced. The turbulent viscosity is normally computed using two transported variables related to the velocity and length scale of turbulence. The most popular choice of variables is the turbulent kinetic energy k and the turbulence dissipation rate ϵ defined as $\epsilon = \nu \overline{u_{i,j} u_{i,j}}$.

In their early forms, both classes of models treat the solid boundary and molecular viscosity effects by using the *wall function* approach[4]. In this method the viscous and buffer layers in the wall proximity are modelled by an algebraic expression that relates the turbulent quantities to the shear velocity under the hypothesis of local equilibrium turbulence. While the assumption is valid for fully developed flow conditions, it is the well known cause of inaccuracies in case of strong streamline curvature, adverse pressure gradients or in stagnation regions that are often encountered in practical flow configurations. The full Reynolds stress models have been applied to the study of an impinging jet in a squared duct [5] with satisfactory agreement with experiments, whereas two equation models have been used for the simulation of a much wider class of flows[1]. Unfortunately, most of the applications have been carried out by the high Re formulations that still retain the wall function approach in presence of solid boundaries to avoid the difficulties connected to the simulation of the viscous and buffer layers.

More recently, with the introduction of new forms, called *low Re*, (LR), of both the full Reynolds stress and two equation models, it is possible to account for the molecular viscosity and the wall effect[6, 7]. The LR forms differ from the standard high Re forms insofar as they include further terms to model the influence of molecular viscosity that is not negligible in wall regions, the normal velocity fluctuation damping exerted by a solid boundary, and the presence of a nonisotropic contribution to the

dissipation rate of turbulence that becomes dominant in the viscous layer. The LR models have been designed to maintain the high Re formulation in the log-law region and further tuned to fit measurements in the viscous and buffer layers. Because of the difficulties in measuring the turbulent stresses in the wall proximity the models have been made to reproduce measurements with a very wide uncertainty range, thereby making turbulence model refinement very unreliable. The recent availability of the results of direct numerical simulation of turbulent flows, even if restricted to very simple flow configurations and quite low Reynolds numbers, helps in understanding the limiting behavior at boundaries of the turbulence quantities and provides a valuable data base for model testing and refinement. With this in mind, it is possible to improve simple models making them consistent with the abovementioned data set.

In this paper the attention will be focused on lower order two-equation models in their LR form. From a computational point of view, the modifications introduced to model the wall effect often cause serious numerical problems so that the results of the computations may be heavily affected by the adopted solver. A comparison of the predictions given by the existing $k - \epsilon$ LR models obtained with a single solver able to cope with all the formulations is definitely desirable and was one of the targets of the present investigation, together with the development of a new general $k - \epsilon$ model. This also allowed investigating the numerical behavior of the models.

2 $k - \epsilon$ LR models

In the current literature it is possible to find several wall effects modifications to the standard high Re $k - \epsilon$ model. Among the various LR formulations nine of them were considered for the comparison with the present model (*pr*) proposed in this paper: Chien[8], (*ch*), Jones and Launder[9], (*jl*), Nagano and Hishida[10], (*nh*), Coakley[11], (*co*), Speziale et al.[12], (*sp*), Kim[13], (*ki*), Rodi[14], (*ro*), Lam and Bremhorst[15], (*lb*), Shih[16], (*sh*). In parentheses are reported the letter codes with which the models will be referred to. The selection was performed on the basis of the results of Patel et al. [6] with the addition of more recent models.

The LR models may be expressed in a standard form in terms of the following nondimensional variables (the overbar stands for a nondimensional quantity):

$$\bar{k} = \frac{k}{U^2} \quad \bar{\epsilon} = \frac{\epsilon L}{U^3} \quad \bar{\nu}_t = \frac{\nu_t}{\nu} \quad \bar{U} = \frac{U}{U} \quad \bar{x}_i = \frac{x_i}{L}$$

in which U is a typical velocity, L is a typical length, and ν is the molecular viscosity. Accordingly, the flow Reynolds number is defined as:

$$Re = \frac{L U}{\nu}$$

Hereinafter the variables will appear only in their nondimensional form so that the overbar will be dropped for simplicity. The model transport equations may be written as follows:

$$\begin{cases} \frac{\partial k}{\partial t} + \frac{\partial U_i k}{\partial x_i} = \frac{1}{Re} \left(\frac{\partial}{\partial x_i} \left(1 + \frac{\nu_t}{\sigma_k} \right) \frac{\partial k}{\partial x_i} \right) + P - \epsilon + D + \Pi \\ \frac{\partial \epsilon}{\partial t} + \frac{\partial U_i \epsilon}{\partial x_i} = \frac{1}{Re} \left(\frac{\partial}{\partial x_i} \left(1 + \frac{\nu_t}{\sigma_\epsilon} \right) \frac{\partial \epsilon}{\partial x_i} \right) + c_1 f_1 \frac{\epsilon}{k} P - c_2 f_2 \frac{\epsilon^2}{k} + E \end{cases} \quad (2)$$

in which

$$P = \frac{1}{Re} \nu_t \left(\frac{\partial U_i}{\partial x_j} \right) \left(\frac{\partial U_j}{\partial x_i} + \frac{\partial U_i}{\partial x_j} \right)$$

is the production rate, and

$$\nu_t = Re c_\mu f_\mu \frac{k^2}{\epsilon} \quad (3)$$

is the Kolmogorov expression for the turbulent viscosity. The extra terms D , E , Π represent the corrections to the standard high Re formulation that, together with the damping functions f_1 , f_2 , f_μ , allow balancing the transport equations (2) in the wall region.

The term D represents the extra destruction rate in the wall region. The dissipation rate appearing in (2) may represent the total dissipation rate, ϵ , or the so called isotropic dissipation rate, $\tilde{\epsilon}$, that are related via the following expression:

$$\epsilon = \tilde{\epsilon} + D \quad (4)$$

in which D is the dissipation budget in the wall region. Evidently, $\epsilon = \tilde{\epsilon}$ far from solid boundaries where $D \rightarrow 0$. A similar correction is generally made in the ϵ transport equation. The extra term Π is the pressure transport term for the trace of the Reynolds stress tensor. Shih[16], analysing the *DNS* computations, observed that Π is $\mathcal{O}(y)$ in the wall region, but is generally neglected in all the existing two-equation models although the turbulent transport is $\mathcal{O}(y^3)$ and remains in the model equation. This term is modeled as a turbulent kinetic energy diffusion.

In all the proposed formulations, the damping functions f_1 , f_μ , are related to the Van Driest damping expression for the mixing length, L :

$$L = y \left(1 - e^{-Ay^+} \right)$$

in which $A = 26$ is an experimental constant, and y^+ is a nondimensional wall distance defined as

$$y^+ = u_\tau y Re \quad (5)$$

The selected transported variables are k and ϵ with two exceptions:

- *co*. The transported variables are $q = \sqrt{k}$ and $\omega = \frac{\tilde{\epsilon}}{k}$. According to Coakley[11], this choice ensures better numerical properties, as explained in ref.[17].
- *sp*. While maintaining k as the first variable, ϵ is replaced by $\tau = \frac{k}{\epsilon}$ in order to remove the inaccuracies connected with the solid wall boundary condition for the dissipation rate, since τ vanishes automatically to zero.

The *ro* two-equation and *ki* four-equation models are *two-layer* models in which an inner layer is defined close to the wall ($y^+ \leq 100$) where, while using a transport equation to compute the turbulent kinetic energy, the dissipation rate is computed by algebraic expressions in function of the wall distance and k . This choice allows removing most of the numerical problems since the cumbersome solution of the dissipation rate equation together with the implementation of a proper boundary condition are skipped in the wall region. Moreover, no extra terms are needed in the transport

model	f_μ	f_1	f_2
<i>ch</i>	$1 - \exp(-.0115y^+)$	1.0	$1 - 0.22\exp(-\frac{R_t^2}{36})$
<i>jl</i>	$\exp\left(\frac{-2.5}{1+\frac{R_t}{50}}\right)$	1.0	$1 - 0.3\exp(-R_t^2)$
<i>nh</i>	$(1 - \exp(-\frac{y^+}{26.5}))^2$	1.0	$1 - 0.3\exp(-R_t^2)$
<i>co</i>	$1 - \exp(-.0065R_y)$	1.0	1.0
<i>sp</i>	$(1 + \frac{3.45}{\sqrt{Re_t}} \cdot \tanh(\frac{y^+}{70}))$	1.0	$1 - 0.22\exp(-\frac{R_t^2}{36})$
<i>ki</i>	$1 - \exp(-.025\sqrt{R_t} - 10^{-5}R_t^2)$	1.0	1.0
<i>ro</i>	$1 - \exp(-.0198R_y)$	1.0	1.0
<i>lb</i>	$(1 - \exp(-.0165R_k))^2 \cdot (1 + \frac{20.5}{R_t})$	$(1 + \frac{.05}{f_\mu})^2$	$1 - \exp(-R_t^2)$
<i>sh</i>	$1 - \exp(-\sum_{i=1}^4 \alpha_i y^{+i})$	1.0	$1 - 0.22\exp(-\frac{R_t^2}{36})$
<i>pr</i>	$1 - \frac{\exp(-.0004 \cdot \exp(1.2R_t^{1/4}))}{\exp(-.0004)}$	1.0	$1 - 0.22\exp(-\frac{R_t^2}{36})$

Table 1: Damping functions in the *LR* forms

model	Π	D	E
<i>ch</i>	0	$-\frac{2}{Re} \frac{k}{y^2}$	$\frac{2\epsilon}{Re y^2} \exp(-.5y^+)$
<i>jl</i>	0	$-\frac{2}{Re} \left(\frac{\partial\sqrt{k}}{\partial y}\right)^2$	$-\frac{2\nu_t}{Re^2} \left(\frac{\partial^2 U}{\partial y^2}\right)^2$
<i>nh</i>	0	$-\frac{2}{Re} \left(\frac{\partial\sqrt{k}}{\partial y}\right)^2$	$-\frac{\nu_t}{Re^2} (1 - f_\mu) \left(\frac{\partial^2 U}{\partial y^2}\right)^2$
<i>co</i>	0	0	-
<i>sp</i>	0	-	-
<i>ki</i>	0	-	-
<i>ro</i>	0	-	-
<i>lb</i>	0	0	0
<i>sh</i>	$\left[\frac{0.05}{f_\mu(1-\exp(-y^+))} \frac{\mu_t}{\sigma_k} k_{,j} \right]_{,j}$	0	$-\frac{\nu_t}{Re^2} \left(\frac{\partial^2 U}{\partial y^2}\right)^2$
<i>pr</i>	$\left[\frac{0.004}{f_\mu^2} \frac{\mu_t}{\sigma_k} k_{,j} \right]_{,j}$	0	$-\frac{\nu_t}{Re^2} \left(\frac{\partial^2 U}{\partial y^2}\right)^2$

Table 2: Extra terms in the *LR* forms

equations since the wall effects are supposed to be effective only within the range of application of the algebraic expression for ϵ .

The damping function expressions selected in the various formulations may be found in table 1, whereas table 2 gives all the selected forms for the extra terms D , E , Π . Most of the models have a set of damping functions based on the physical, y , or nondimensional, y^+ , distance, and on the turbulent Reynolds number based on y , $Re_y = \sqrt{k} y Re$, or $Re_t = \frac{k^2 Re}{\epsilon}$. The exponential function f_μ introduced in (3) damps the turbulent viscosity to zero in the viscous and buffer layers. It is interesting to observe that nearly all the models retain the exponential function for the decay of dissipation rate f_2 proposed by Hanjalic and Launder[18], according to which c_2 has a finite value at the wall. The *sp* formulation needs an additional function to further damp the value of c_2 in the wall region (see ref.[12]). The empirical constant c_1 is left unchanged all the way down to the wall in all the formulations with the only exception of *lb* where, since no extra terms are added in both k and ϵ , the production of dissipation rate must be damped to balance ϵ at the wall.

For any further detail about the models, the reader can refer to the original bibliography.

3 A new form independent of wall distance

The results of *DNS* have shown the limiting forms of the turbulent quantities in the wall region. A correct formulation should ensure that

$$\begin{aligned} U &= o(y) & k &= o(y^2) & \epsilon &= o(1) \\ \bar{\epsilon} &= o(y^2) & \mu_t &= o(y^3) & \overline{uv} &= o(y^3) \end{aligned}$$

together with a negative slope of the dissipation rate in the wall region. The two-equation model proposed by Shih[16] matches the flow variables limiting forms remarkably well, but in its original formulation suffers from numerical problems stemming from the selected form of both the dissipation rate decay term and turbulent viscosity formula. In fact, the dissipation decay rate is

$$-c_2 f_2 \frac{\epsilon \bar{\epsilon}}{k} \quad (6)$$

that is $o(1)$ at the wall, and the turbulent viscosity is computed as

$$\nu_t = c_\mu f_\mu Re \frac{k^2}{\bar{\epsilon}} \quad (7)$$

in which the damping function f_μ is based on a fourth order polynomial of y^+ designed to match the *DNS* data. The isotropic dissipation rate is computed as

$$\bar{\epsilon} = \epsilon - \frac{\left(\frac{\partial k}{\partial y}\right)^2}{2 k Re} \quad (8)$$

This expression ensures that $\bar{\epsilon}$ vanishes at the wall like y^2 , provided that a proper boundary condition makes ϵ equal to the negative term in (8). Even in the computation of simple fully developed channel flows some convergence problems were encountered, which were caused by the decay term given by equation (6). When computing the isotropic dissipation rate with equation (8) the ratio of the first order derivative of k and \bar{k} in the wall region often gives overshoots that cause negative dissipation rates and, through equation (7), negative ν_t .

Alternatively $\bar{\epsilon}$ may be defined as

$$\bar{\epsilon} = \epsilon f_\epsilon \quad (9)$$

where we have introduced a function f_ϵ which is a function of the turbulent Reynolds number, $R_t = \frac{k^2 Re}{\epsilon}$:

$$f_\epsilon = f(R_t) = 1 - \exp(-\sqrt{R_t})$$

At the wall, $R_t = o(y^4)$ so that the function f_ϵ is $o(y^2)$. Equation (9) prevents any negative dissipation rate, makes $\bar{\epsilon} = o(y^2)$ at the wall, and is balanced by molecular diffusion and the extra production rate E . The f_ϵ function is designed to give $\bar{\epsilon} \approx \epsilon$ for $y^+ \geq 6$.

Table 1 shows that all the *LR* forms except the *jl* model use damping functions for ν_t based on y or y^+ , while f_2 is based on R_t . The use of y^+ as the exponent of the damping functions gives unphysical results in the case of stagnation points. In fact, the definition of the *friction velocity* u_τ appearing in equation (5) is:

$$u_\tau = \sqrt{\frac{\tau_{wall}}{\rho}}$$

$$\tau_{wall} = \mu_{lam} \left(\frac{\partial U}{\partial n} \right)_{wall}$$

where n is the direction normal to the wall. At separation and reattachment points

$$\left(\frac{\partial U}{\partial n} \right)_{wall} \rightarrow 0$$

and $y^+ \rightarrow 0$ regardless of the value of y . This implies that f_μ is zero all along the flow section making the viscous layer thickness unphysically unbounded. There are several known *tricks* to overcome this problem, like relating u_τ to the k peak in the viscous layer via the wall function for the turbulent kinetic energy:

$$u_\tau \approx \sqrt{\sqrt{c_\mu} k_{max}},$$

or replacing the velocity gradient by the maximum value of the vorticity ω in the cross flow direction:

$$\left(\frac{\partial U}{\partial n} \right)_{wall} \approx |\omega_{max}|$$

While these, and other, tricks remove the singularity, they are somewhat arbitrary and represent sources of inaccuracy. Moreover, a general turbulence model should

not need information about the flow domain geometry, like the wall distance, the determination of which is not straightforward in complex geometries. Unfortunately, replacement of y^+ is not an easy task. In fact, while f_2 becomes constant for $y^+ \geq 5 - 10$, f_μ , related to the wall effects, vanishes gradually in the range $0 \leq y^+ \leq 100$. Figure (1) shows the R_t profile as a function of y^+ : the turbulent Reynolds number increases very steeply for $0 \leq y^+ \leq 50$, reaches a peak at $y^+ \approx 80$ and decreases for $y^+ \geq 100$. When keeping as a benchmark the $f_\mu = f(y^+)$ given in [16], which was carefully designed to give the best fit with *DNS*, it has been impossible to replace y^+ by R_t even using complicated hyperbolic expressions because the turbulent Reynolds number does not behave monotonically. After intense numerical testing we found convenient to introduce a new damping function independent of y and based on length scales. Figure (2) shows that the turbulence length scale, defined as

$$L = \frac{k^{\frac{3}{2}}}{\epsilon}$$

or

$$\bar{L} = \frac{k^{\frac{3}{2}}}{\bar{\epsilon}}$$

has a monotonic behavior so that it may be conveniently used to replace y^+ . A new nondimensional parameter, R_L , based on L is introduced:

$$R_L = \frac{L}{L_\nu} \quad (10)$$

in which

$$L_\nu = \frac{\nu}{|U|}$$

$|U|$ is the amplitude of the relative mean velocity in a frame fixed to the solid boundary. This choice ensures the Galileian invariance of the model equations. R_L represents the ratio of the turbulence length scale L to the viscous length scale L_ν . This ratio approaches zero at the wall because $L \rightarrow 0$, $L_\nu \rightarrow \infty$, and reaches asymptotically a maximum in the log-law region. In the wall region the following limiting forms hold:

$$\left. \begin{array}{l} L = o(y^3) \\ U = o(y) \end{array} \right\} \rightarrow R_L = o(y^4)$$

Accordingly, the exponent of the damping expression must be $R_L^{\frac{1}{4}}$ to give $f_\mu = o(y)$ at the wall. The new damping function based on (10) has the following expression:

$$f_\mu = 1 - \frac{1}{\exp(-c_{\mu 1})} \cdot \exp\left(-c_{\mu 1} \exp\left(c_{\mu 2} R_L^{1/4}\right)\right) \quad (11)$$

in which $c_{\mu 1}$ and $c_{\mu 2}$ are two empirical constants. The f_μ function given by Shih[16] versus $R_L^{\frac{1}{4}}$ is shown in figure (3). The shape of the exponent of $f_\mu (= -\ln(1 - f_\mu))$

closely resembles an exponential: this was the reason why a double exponential function was selected.

Figure (4) shows that the differences between the original damping function[16] and the new form are limited to the viscous layer ($y^+ \leq 10$), while in the buffer and log-law region the new form independent of the wall distance quite closely resembles the formulation based on the nondimensional wall distance.

With the substitution of equation(8) by equation (9) and the replacement of the damping function for the turbulent viscosity by equation(11), a new model tuning was necessary. In the present formulation Π has the form given in table 2, $c_1 = 1.45$, $c_2 = 2.0$, $\sigma_k = \sigma_\epsilon = 1.3$, $c_{\mu 1} = 0.4 \cdot 10^{-3}$, $c_{\mu 2} = 1.2$. The boundary condition for the dissipation rate is

$$\epsilon_{wall} = \frac{\left(\frac{\partial k}{\partial y}\right)^2}{2 k Re} \quad (12)$$

4 Fully developed turbulent channel flow

Patel et al. [6], while comparing some LR forms with experiments, stressed the data unreliability in the wall proximity in the range $0 < y^+ < 100$. In this region the scatter in the turbulent kinetic energy k is of the order of $\pm 30\%$, and comparable inaccuracies may be expected for the turbulent shear stress \overline{uv} , defined in equation (1), and the dissipation rate ϵ . Because of these uncertainties it was decided to use the direct numerical simulation results of a fully developed channel flow by Mansour et al.[3] at $Re = 3300$ based on the maximum velocity, or $Re_\tau = 180$ based on the friction velocity. All the derivatives in the flow direction are zero, with the exception of the streamwise pressure gradient that is constant. This allowed studying the problem by a one dimensional grid with 81 points in the cross flow direction and a geometric stretching ratio of 1.05. With this grid it was possible to place the first grid point away from the wall at $y^+ \approx 0.15$. The transport equations are nondimensionalized with respect to half channel height and the friction velocity u_τ , while the turbulent viscosity is made nondimensional with respect to the laminar viscosity ν . The domain and the solution are symmetric with respect to the centerline where the following boundary conditions were imposed:

$$\frac{\partial U}{\partial y} = \frac{\partial k}{\partial y} = \frac{\partial \epsilon}{\partial y} = 0$$

Under these assumptions continuity is automatically satisfied and the momentum equation in the main flow direction, x , is simplified to:

$$\frac{\partial U}{\partial y} = Re_\tau \left(\frac{1-y}{1+\nu_t} \right)$$

in which y represents the cross flow direction and U is the flow velocity. The transport equations for k and ϵ become:

$$\begin{cases} \frac{1}{Re_\tau} \left(\frac{\partial}{\partial y} \left(1 + \frac{\nu_t}{\sigma_k} \right) \frac{\partial k}{\partial y} \right) + P - \epsilon + D + \Pi = 0 \\ \frac{1}{Re_\tau} \left(\frac{\partial}{\partial y} \left(1 + \frac{\nu_t}{\sigma_\epsilon} \right) \frac{\partial \epsilon}{\partial y} \right) + c_1 f_1 \frac{\epsilon}{k} P - c_2 f_2 \frac{\epsilon^2}{k} + E = 0 \end{cases}$$

in which the one dimensional production rate is expressed by:

$$P = \frac{1}{Re_\tau} \nu_t \left(\frac{\partial U}{\partial y} \right)^2$$

The differential system is solved by a decoupled approach based on a simplified approximate factorization algorithm described in ref.[2, 17]. The comparison of the various models is done by plotting the mean velocity U , the turbulent kinetic energy k , the dissipation rate ϵ , the turbulent shear stress \overline{uv} , the turbulent viscosity ν_t , and the production rate P . The plots gather models that solve for the isotropic dissipation rate $\bar{\epsilon}$, (*ch, jl, nh*), models that use a different set of variables (*co, sp*), two-layer models (*ki, ro*), and models that solve for the total dissipation rate (*lb, sh, pr*). The *sh* results reported here have been obtained with a slightly modified version of the model in which the original expression for $\bar{\epsilon}$ given in equation (8) was replaced by equation (9).

Figure 5 shows the computed velocity profiles compared with *DNS*, whereas figure 6 shows the comparison of the turbulent viscosity profiles. Among the models that solve for the isotropic dissipation rate *nh* is the one in better agreement with *DNS*. This is strictly related to the good reproduction of the turbulent viscosities in the viscous and buffer layers. This produces the correct velocity gradient in the buffer layer together with a slight overprediction of the centerline velocity. The good agreement is obtained by *nh* despite the fact that, at the wall, $\nu_t = o(y^4)$ because $f_\mu = o(y^2)$. *jl* gives a strong underestimation of the centerline velocity. This is caused by the underestimation of the turbulent viscosity in the buffer layer that does not ensure enough cross flow momentum diffusion. The reason for this is the damping function for the turbulent viscosity f_μ . This function, designed to work for high *Re* flows, in this case does not reach unity for $y^+ \geq 100$ and is still approximately 0.65 on the centerline. This exceedingly smooth behavior indicates that the selected form of the damping function for the turbulent viscosity, while being based on R_t and not on y^+ , is not general. *sp* shows an excellent agreement with experiments (figure 5). This is strictly linked with the good reproduction of the turbulent viscosity profile (figure 6). In fact, *DNS*[3] and experiments[19] agree in locating the peak of turbulent viscosity at $100 \leq y^+ \leq 150$ and not on the centerline: this feature is correctly reproduced by *sp*, while is completely missed by *co* in which the overestimation of the turbulent viscosity causes a very smooth and overpredicted velocity. For the two-layer models the influence of the matching point was investigated. For *ro* the two computations carried out matching at $y^+ = 50$ and $y^+ = 100$ showed a considerable change in the turbulent viscosity, but negligible changes in all the other quantities including the velocity profile. The four-equation, two-layer *ki* model retains f_μ only in the inner layer, while it assumes that in the outer layer $f_\mu = 1$. The selected form of the damping function seems to suffer the same problems encountered with *jl* insofar as at matching ($y^+ = 100$) the damping function is still 0.7. This is shown in figure 6 where *ki* refers to the original formulation by Kim[13], while in *ki(fmu)* the damping function was retained in the outer layer. As it was found for *ro*, the velocity profile is not affected by changes in turbulent viscosity taking place at $y^+ \geq 100$. The three models that solve for ϵ give the best overall agreement with the *DNS* velocity profile. The present formulation, *pr*, fits with *DNS* in the buffer layer, and predicts the correct velocity at the centerline. The improvement with respect to *jl*, which is

the only other model that does not use the wall distance, is quite remarkable. The ν_t profile exhibits the correct trend, although the turbulent viscosity value is slightly overpredicted on the centerline.

The turbulent kinetic energy profiles, reported in figure 7, show a quite wide scatter in the computational results. For all the models $k \propto y^2$ at the wall. Nevertheless the k peak is either misplaced or underpredicted. An accurate choice of the constant in the pressure transport term together with a correct dissipation rate budget in the wall region allows the *sh* and *pr* formulations to fit both the location and the magnitude of the turbulent kinetic energy maximum value, although the k level in the log-law region, which influences the turbulent viscosity distribution, is overestimated. Both the two-layer forms do not seem to match the data not only in the region of application of the algebraic expression for ϵ , but also in the outer layer. *sp*, while giving an exceedingly low k peak, predicts the correct level of turbulent kinetic energy in the log-law region.

The turbulent shear stress profiles are given in figure 8. This quantity is critical for the correct reproduction of the effect of turbulence on the mean flow field. Not all the models satisfy the relation $\overline{uv} \propto y^3$ at the wall. In particular, *nh*, *co*, and *lb* predict $\overline{uv} \propto y^4$. Since all the models ensure $U^+ \propto y^+$ the disagreement is caused by an improper slope of the turbulent viscosity induced by the damping functions. When both k and $\tilde{\epsilon}$ are $o(y^2)$, f_μ must be $o(y)$: the latter condition is not satisfied by *nh* and *co*, in which $f_\mu = o(y^2)$, while for *lb* the inaccuracy comes from $f_\mu = o(1)$ together with the use of the total dissipation rate $\epsilon = o(1)$ to compute the turbulent viscosity. *sp* and *pr* show the best fit with experiments. Nevertheless the present formulation manages to give the proper \overline{uv} shape. This has been accomplished by optimization of the $c_{\mu 1}$ and $c_{\mu 2}$ constants.

Both the two-layer models show a *kink* in the turbulent shear stress profile located at the interface between the inner and the outer layers. The kink is caused by an imperfect match between the inner layer, where an algebraic expression for ϵ holds, and the outer layer where the standard high Re transport equation for ϵ is implemented. The two layers are normally interfaced in such a way that the value of the dissipation rate obtained by the algebraic expression equals the one obtained by the transport equation. At the interface point the two layers may have the same ϵ value, but evidently have slightly different slopes that induce the kink. Different damping functions, choice of constants, and matching criteria did not solve the problem, so that it is reasonable to conclude that, up to now, it has been not possible to ensure a $C1$ continuity for ϵ at the matching point, and it is actually questionable whether it is possible. In the elliptic flow solver based on *tl*[2] the layers were matched where $\nu_t/\nu \approx 20 - 36$. In the present low Re flow, this condition is never satisfied so that the layers are matched according to the nondimensional wall distance y^+ . Part of the inaccuracies shown by *tl* may be attributed to this technique which brings the matching point too close to the wall.

DNS shows that the ϵ peak is located at the wall and the slope of the dissipation rate is negative in the viscous layer. These two results contradict what have been found so far by experiments. The reason for this disagreement is largely attributed to difficulties in measuring turbulent velocity gradients close to the wall with the result of an extremely large experimental uncertainty. All the older formulations have been tuned to have a positive or zero ϵ slope at the wall. The only models that took advantage of *DNS* are *sp*, *sh*, and the present formulation: this should be kept in

mind when looking at the results. Figure 9 shows the dissipation rate profiles for the ten models. For the formulations that solve for $\bar{\epsilon}$ the plots refer to the isotropic dissipation rate without the extra dissipation D (equation 4). This term, while being dominant in the viscous layer, gives values of ϵ at the wall that are at most half of what DNS prescribes, together with a positive slope. The local peak of dissipation rate away from the wall takes place at $y^+ \approx 12$ and is not influenced by the extra term D which decays very quickly and is not negligible in the range $0 \leq y^+ \leq 10$. In all the models, including sp , sh and pr there is a marked tendency to overestimate this peak, with the exception of ch which fits very well with DNS in the range $10 \leq y^+ \leq 180$, probably because of the selected form of the extra production term E . The only two models that exhibit the correct dissipation rate slope at the wall are sh and the present formulation pr based on the sh model. The correction adopted to the isotropic dissipation rate formula in sh , based on an exponential damping function, while removing numerical troubles, produces an overestimation of ϵ at the wall of the order of 2.5 times the value given by DNS . Although $\bar{\epsilon}$ is $o(y^2)$ at the wall, it seems that it has been not possible to obtain the proper balance between the molecular diffusion of dissipation and decay rate. The problem may be generated by the difficulties in the implementation of a proper boundary condition for ϵ . In fact, the dissipation rate must reach a finite value at the wall which comes from the balance of the abovementioned terms. The errors in computing first or second order derivatives at the wall may be the primary source of inaccuracies in the treatment of solid boundaries. The dissipation rate boundary condition given in equation (12) was retained for both sh and pr . The overestimation of the wall value of ϵ is reduced to 40% by the present formulation. It has to be observed that sh and pr are the only models, among those considered in this comparison, that show a negative ϵ slope at the wall.

Figure 10 proves the close link between the velocity profiles, together with the turbulent shear stress, and the production rate P . The plots show that the models locating P_{max} at $y^+ \approx 10 - 11$ reproduce very well the velocity profile. If P_{max} , regardless of its value, is located at $y^+ \leq 10$ the velocity module on the centerline will be underestimated, while shifting P_{max} further out generally produces an overestimation.

5 Conclusions

A new $k - \epsilon$ LR model is presented. The formulation was obtained starting from the LR form proposed by Shih[16]. The comparison of the new formulation together with nine other LR forms shows an overall improvement in the fit with the direct numerical simulation data. The lower order model generality is greatly improved by introducing a new damping function for the turbulent viscosity which does not need information about the flow geometry. This is done by a new form of f_μ based on the ratio of the turbulent and viscous length scales R_L that removes the uncertainties and inaccuracies stemming from the need to define a geometrical distance from solid boundaries. It is necessary to test the new formulation independent of y^+ for a wide range of Reynolds number and geometries. Further work is on the way to extend the comparison to elliptic flows, focusing the attention on those models that proved to possess the necessary degree of generality.

Some of the models, like the two-layer formulations, showed a poor fit with ex-

periments. This is not surprising since these, and other, models had been tuned to fit high- Re flows using different data sets. Most of these formulations proved to give satisfactory depictions of more complex flow patterns than the one investigated here. Nevertheless, the comparison of the models in such a simple, and ideal, flow case allowed highlighting some differences that would have probably been lost in a complex flow configuration.

Acknowledgment

This work was carried out at the Institute for Computational Mechanics in Propulsion, NASA Lewis Research Center, the support of which is gratefully acknowledged.

References

- [1] Rodi, W.: Turbulence Models and their Application in Hydraulics. International Association of Hydraulic Research, Monograph, Delft, The Netherlands, 1980.
- [2] Michelassi, V.: Testing of Turbulence Models with an Artificial Compressibility Solution Method. Report SFB (Sonderforschungsbereich, University of Karlsruhe) 210 T49, University of Karlsruhe, Karlsruhe, West Germany, January 1989.
- [3] Mansour N.N.; Kim J.; and Moin P.: Reynolds-stress and Dissipation-Rate Budgets in a Turbulent Channel Flow. *Journal of Fluid Mechanics* Vol. 194, 1988, pp.15-44.
- [4] Launder, B.E.; Spalding, D.B.: The Numerical Computation of Turbulent Flows. *Comp. Math. App. Mech. Engg.*, Vol. 3, 1974, pp.269-289.
- [5] Demuren, A.O.: Calculation of 3D Turbulent Jets in Crossflow with a Multigrid Method and a Second-Moment Closure Model. NASA TM-103159, ICOMP-90-15, 1990.
- [6] Patel, V.C.; Rodi, W.; and Sheuerer, G.: Turbulence Models for Near-Wall and Low Reynolds Number Flows: A Review. *AIAA Journal*, Vol. 23, no. 9, 1985, pp. 1308-1319
- [7] Shih T.-H.; Mansour N.N.: Modeling of Near-Wall Turbulence. *Proceedings of the International Symposium on Engineering Turbulence Modelling and Measurements*, September 24-28, 1990, Dubrovnik, Yugoslavia.
- [8] Chien, K.Y.: Predictions of Channel and Boundary-Layer Flows with a Low-Reynolds-Number Turbulence Model. *AIAA Journal*, Vol. 20, no.1, 1982, pp. 33-38.
- [9] Jones, W.P.; Launder, B.E.: The Calculation of Low-Reynolds Number Phenomena with a Two-Equation Model of Turbulence. *International Journal of Heat and Mass Transfer*, Vol.16, 1973, pp. 1119-1130.
- [10] Nagano, Y.; Hishida, M.: Improved Form of the $k - \epsilon$ Model for Wall Turbulent Shear Flows. *ASME Transactions, Journal of Fluid Engineering*, Vol. 109, 1987.

- [11] Coakley, T.J.: Turbulence Modelling Methods for the Compressible Navier-Stokes Equations. *AIAA paper* 83-1693, 1983.
- [12] Speziale, C.G.; Abid, R.; and Anderson, E.C.: A critical Evaluation of Two-Equation Models for Near Wall Turbulence. *AIAA paper* 90-1481, 1990.
- [13] Kim, S.-W.: Near-Wall Turbulence Model and its Application to Fully Developed Turbulent Channel and Pipe Flows. *Numerical Heat Transfer, Part B, Vol.17*, 1990, pp. 101-122.
- [14] Rodi, W.: Recent Developments in Turbulence Modelling. *Proceedings, Third International Symposium on Refined Flow Modelling and Turbulence Measurements*, July 1988, Tokyo, Japan.
- [15] Lam, C.K.G.; Bremhorst, K.: A Modified Form of the $k - \epsilon$ Model for Predicting Wall Turbulence. *Transaction of the ASME, Journal of Fluids Engineering, Vol.103*, September 1981, pp. 456-460.
- [16] Shih, T.H.: An Improved $k - \epsilon$ Model for Near-Wall Turbulence and Comparison with Direct Numerical Simulation. NASA TM-103221, ICOMP-90-16, 1990.
- [17] Michelassi, V.; Martelli F.: Numerical Computation of Turbulent Flows by Low-Reynolds-Number Two-Equation Models. *Proceedings of the International Symposium on Engineering Turbulence Modelling and Measurements*, September 24-28, 1990, Dubrovnik, Yugoslavia.
- [18] Hanjalic, K.; Launder, B.E.: Contribution Towards a Reynolds Stress Closure for Low-Reynolds-Number Turbulence. *Journal of Fluid Mechanics* Vol. 74, 1976, pp.593-610.
- [19] Naot, D.; Rodi, W.: Numerical Simulation of Secondary Currents in Open Channel Flow with an Algebraic Stress Turbulence Model. Report SFB (Sonderforschungsbereich, University of Karlsruhe) 80/T/187, University of Karlsruhe, Karlsruhe, West Germany, 1981.

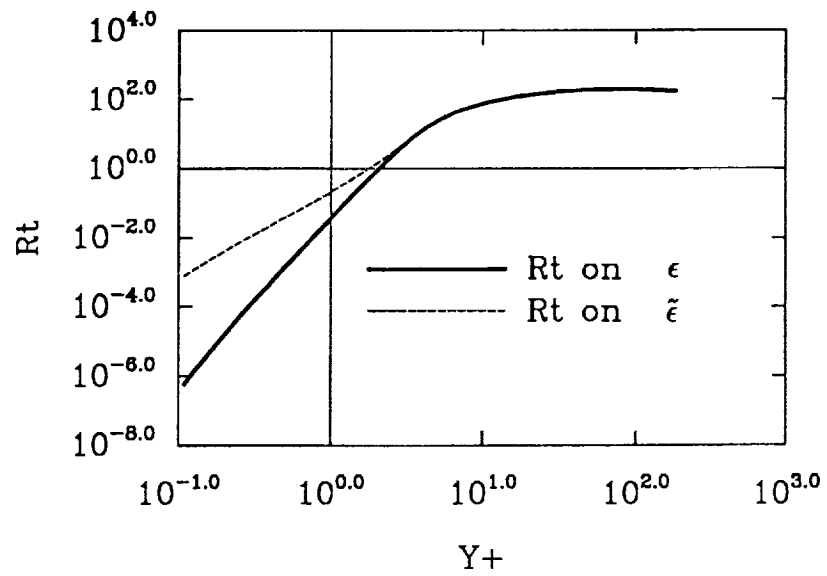


Figure 1: Turbulent Reynolds number profile

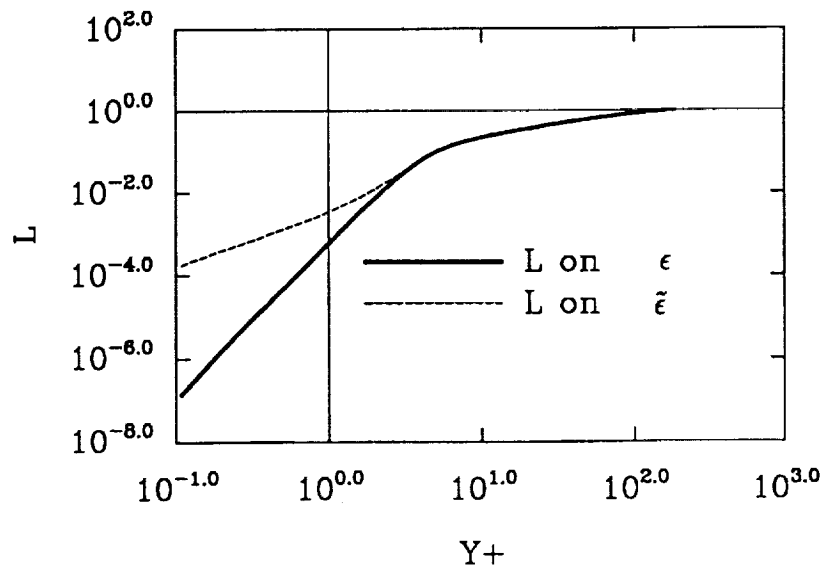


Figure 2: Turbulence length scale

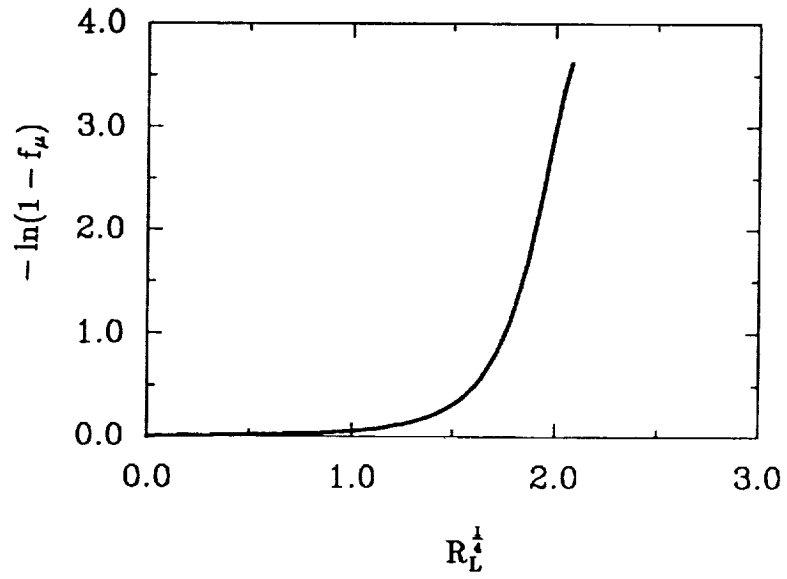


Figure 3: f_μ in function of $R_L^{1/4}$

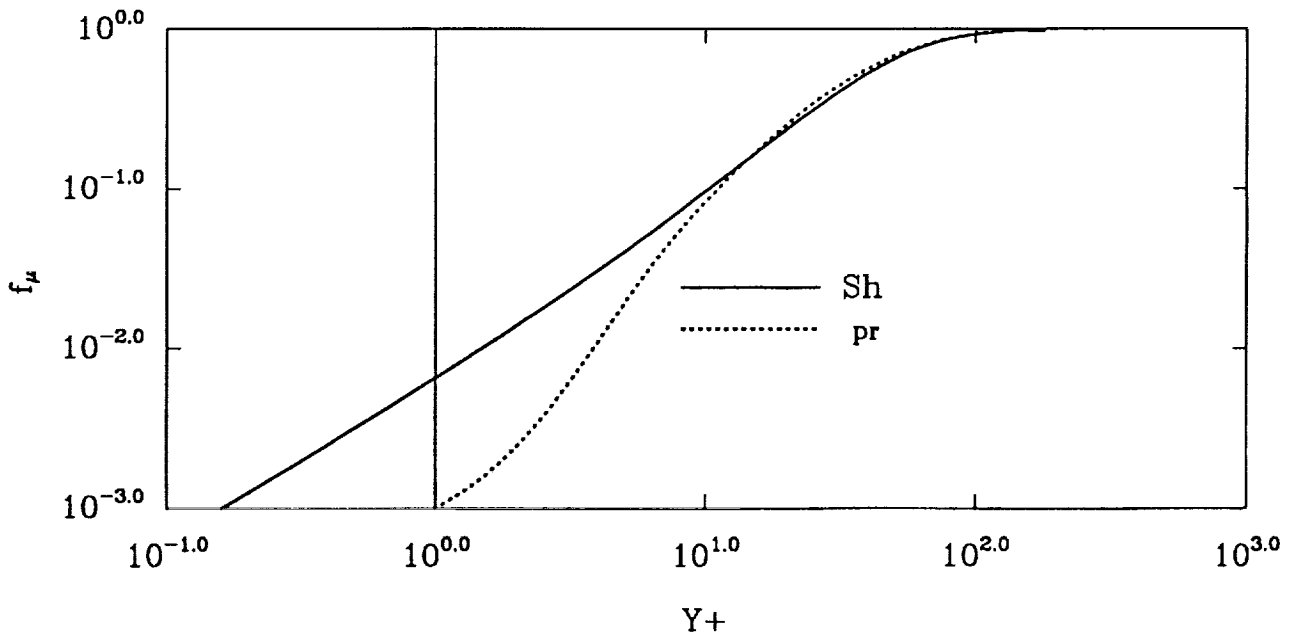


Figure 4: f_μ based on y^+ and R_L

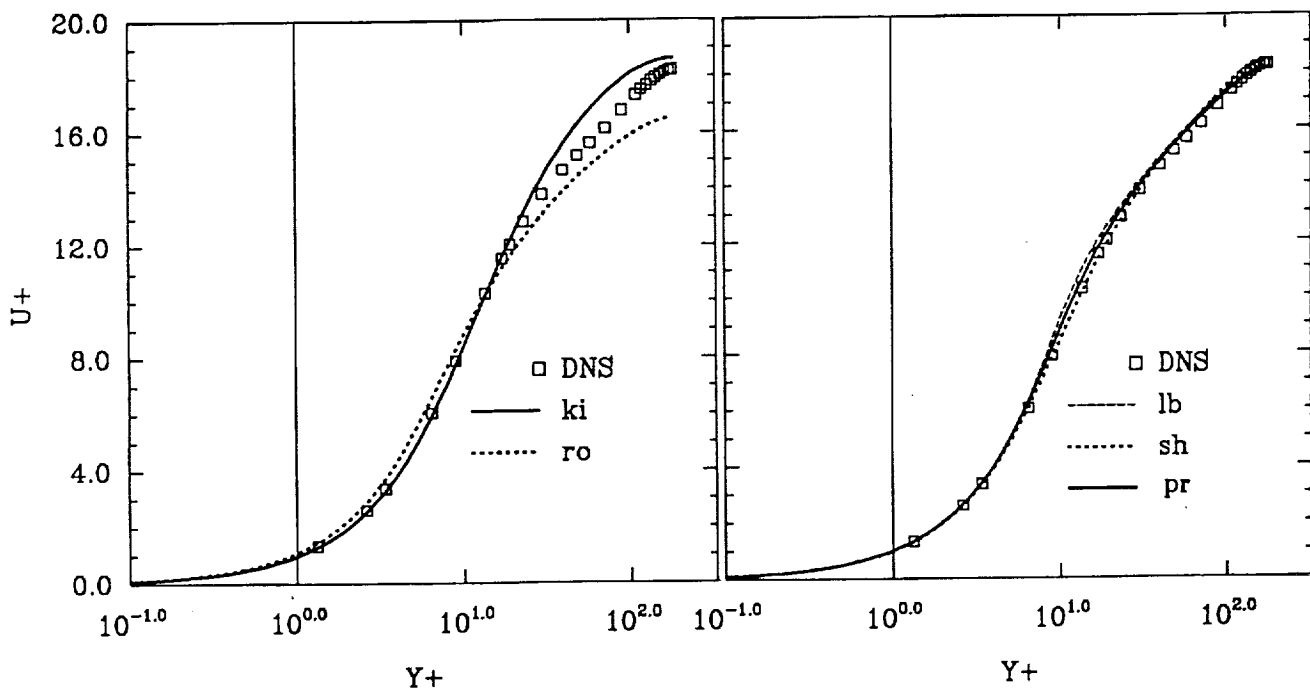
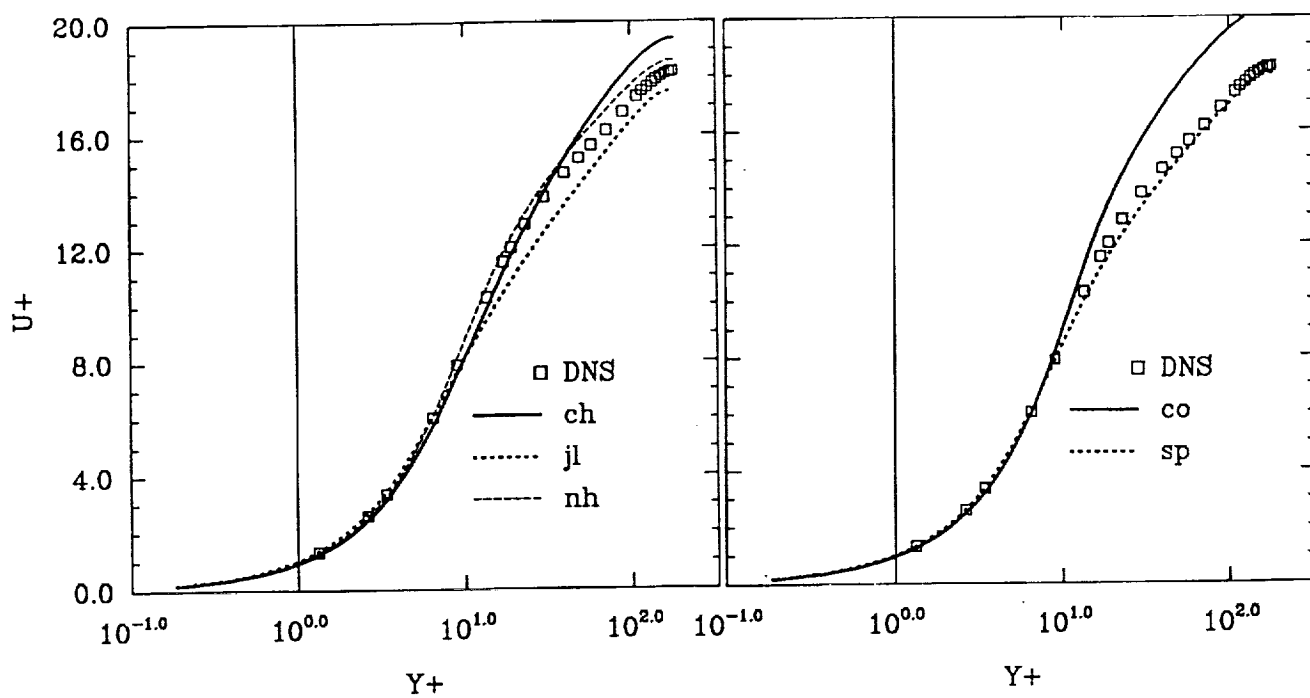


Figure 5: Mean velocity profiles

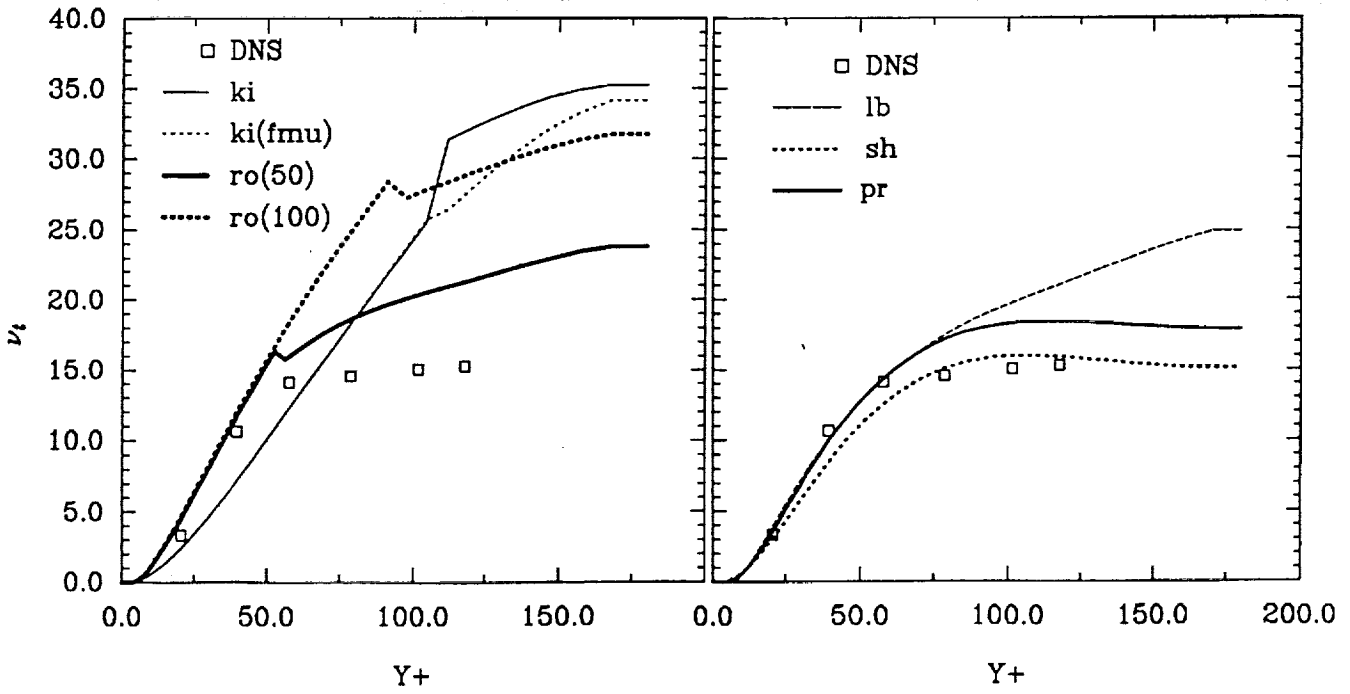
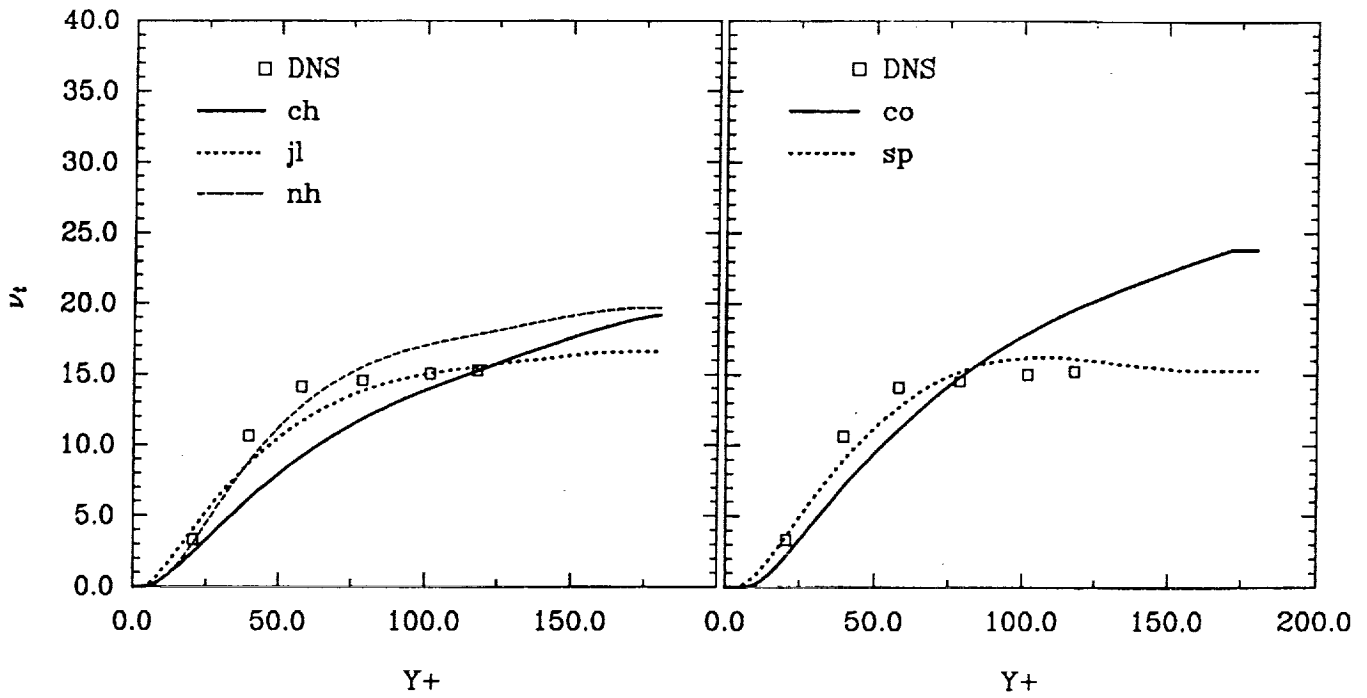


Figure 6: Turbulent viscosity profiles

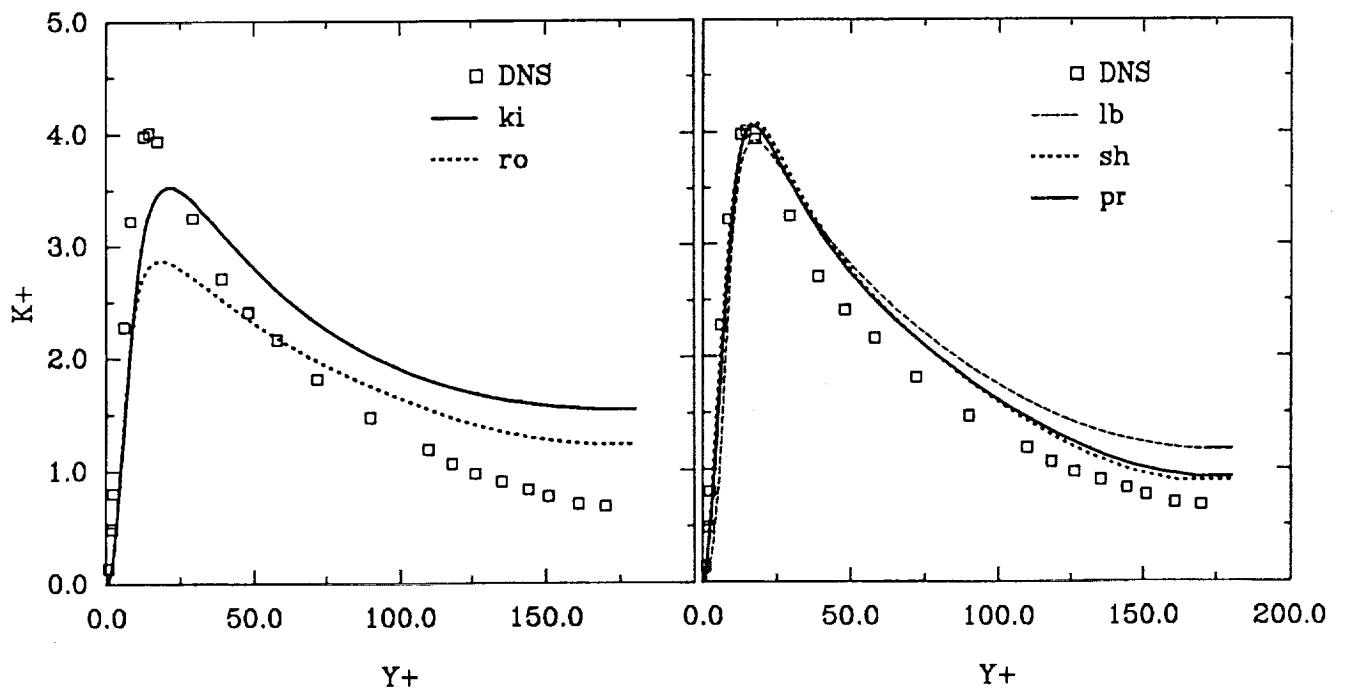
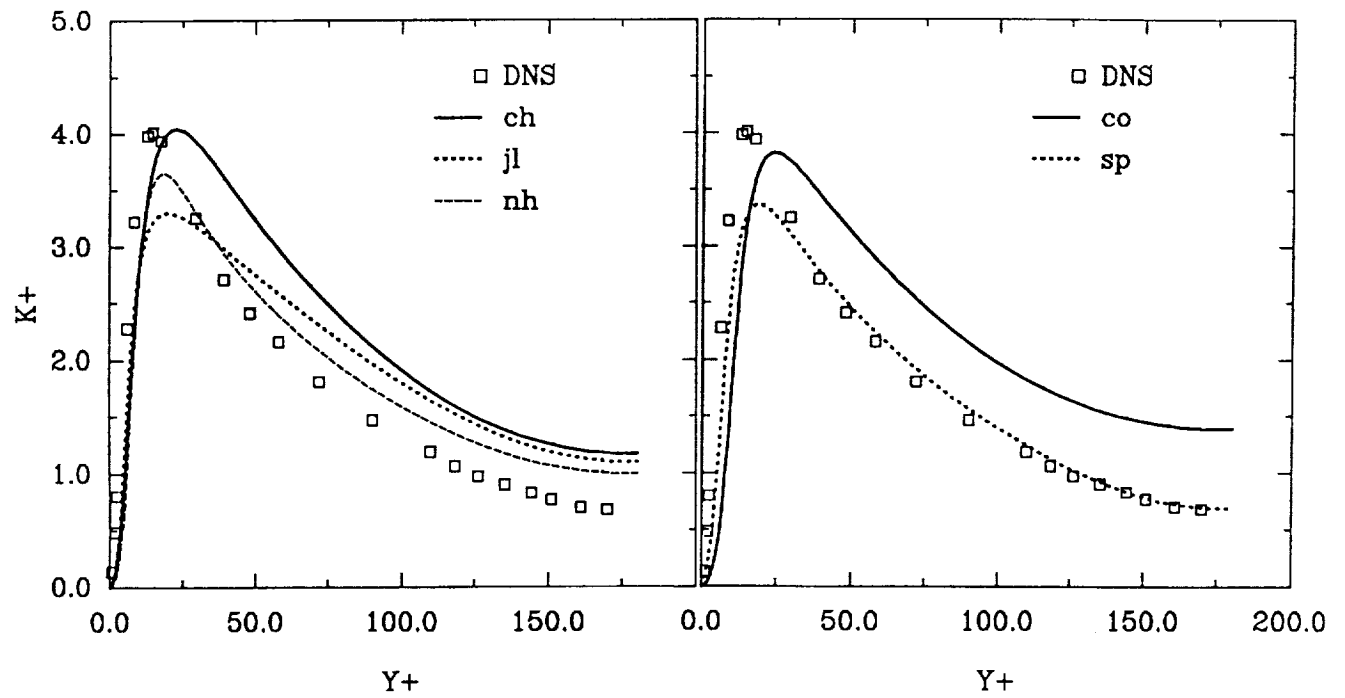


Figure 7: Turbulent kinetic energy profiles

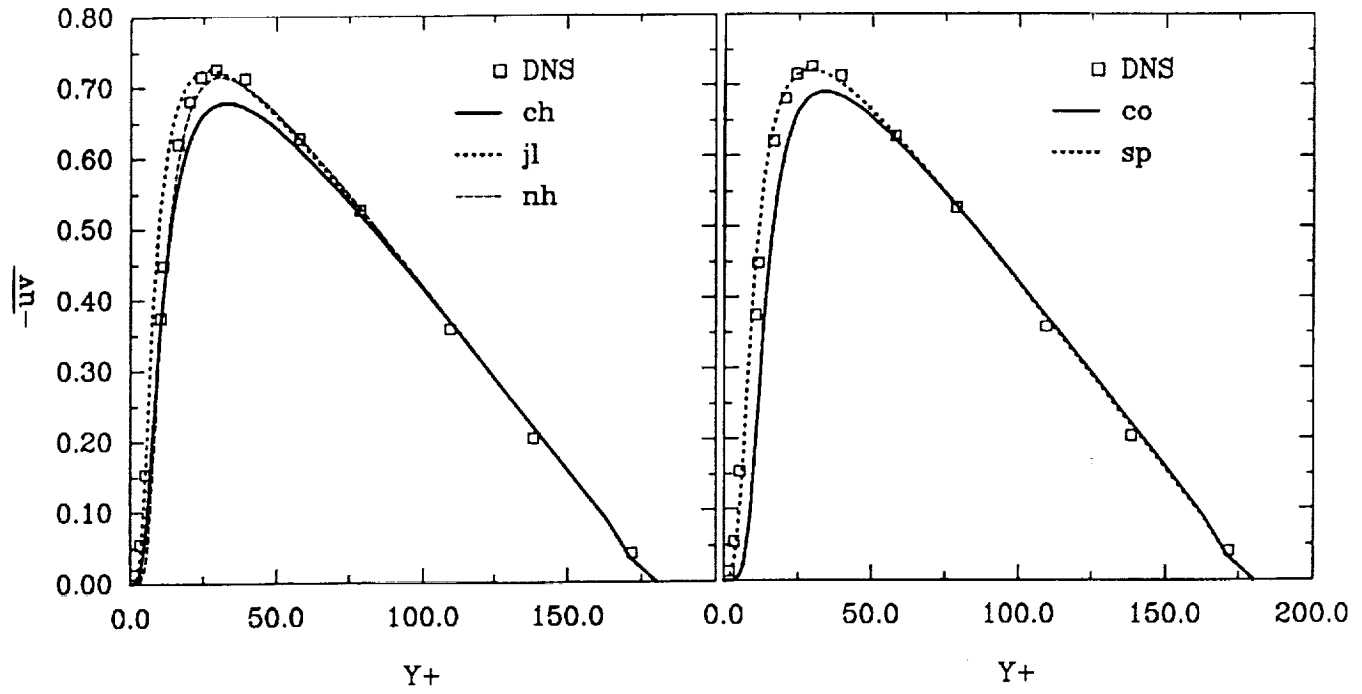


Figure 8: Turbulent shear stress profiles

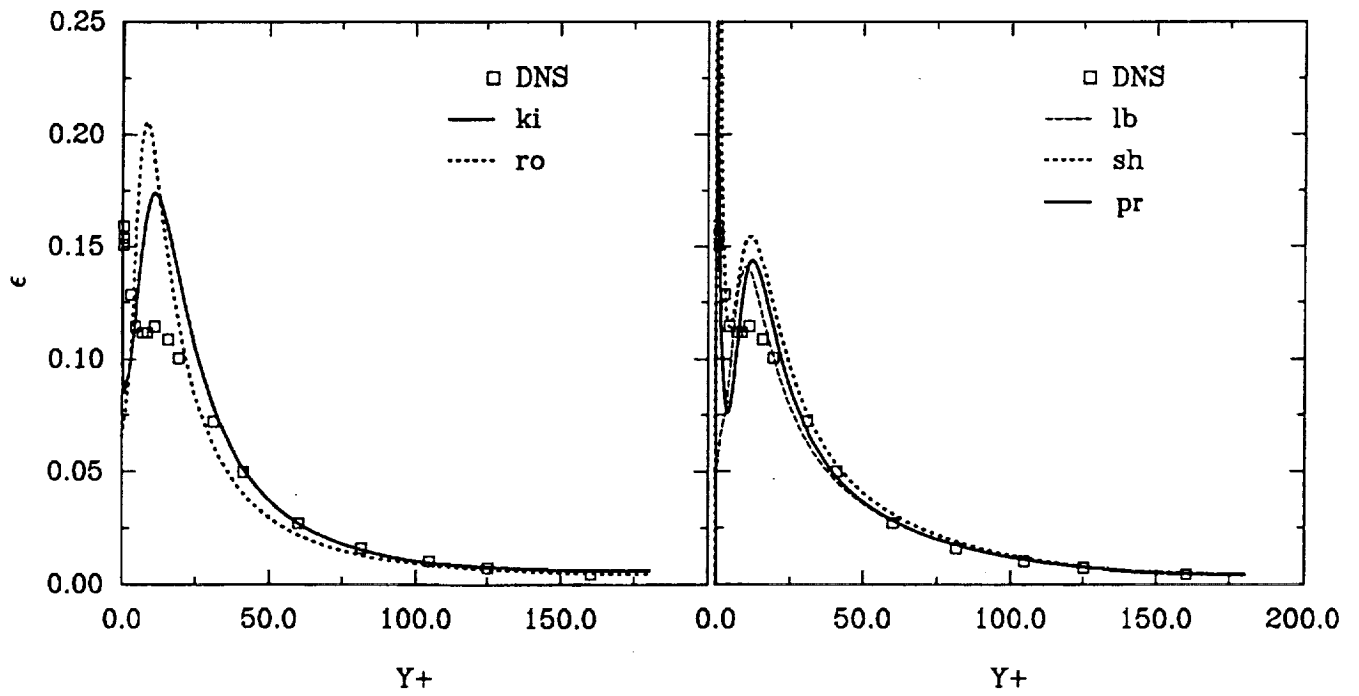
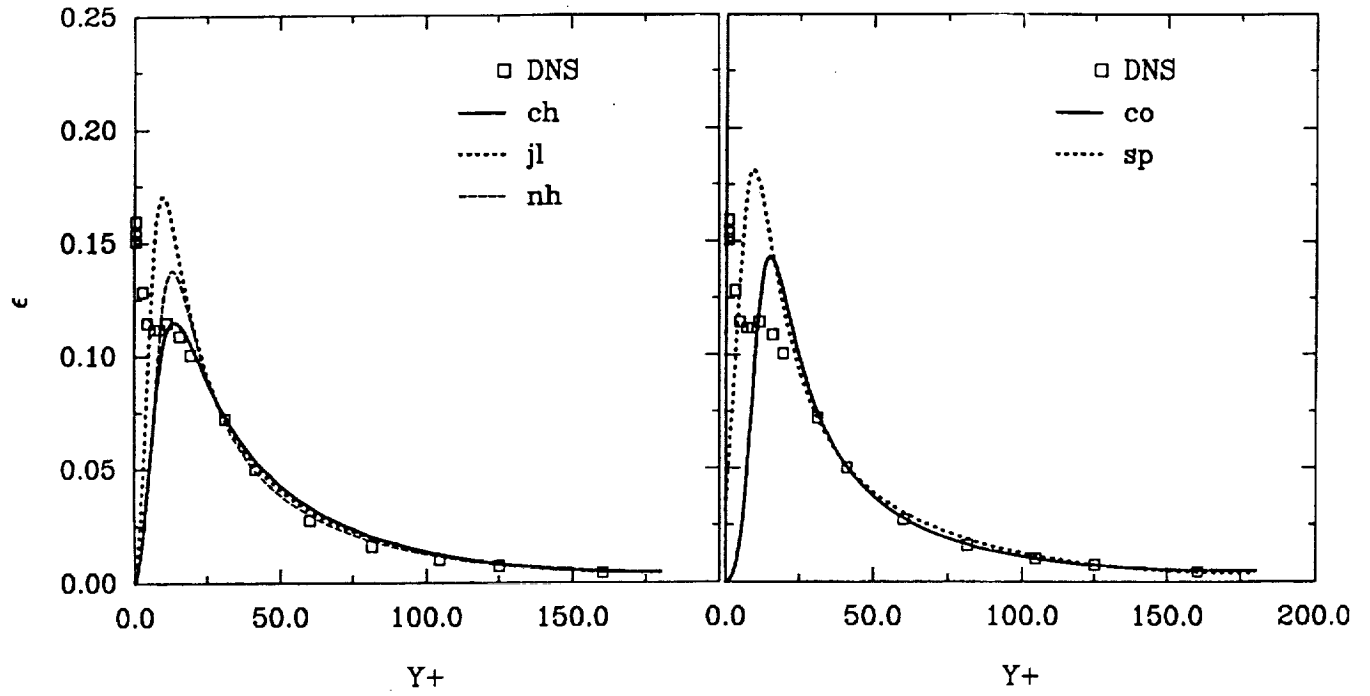


Figure 9: Turbulent dissipation profiles

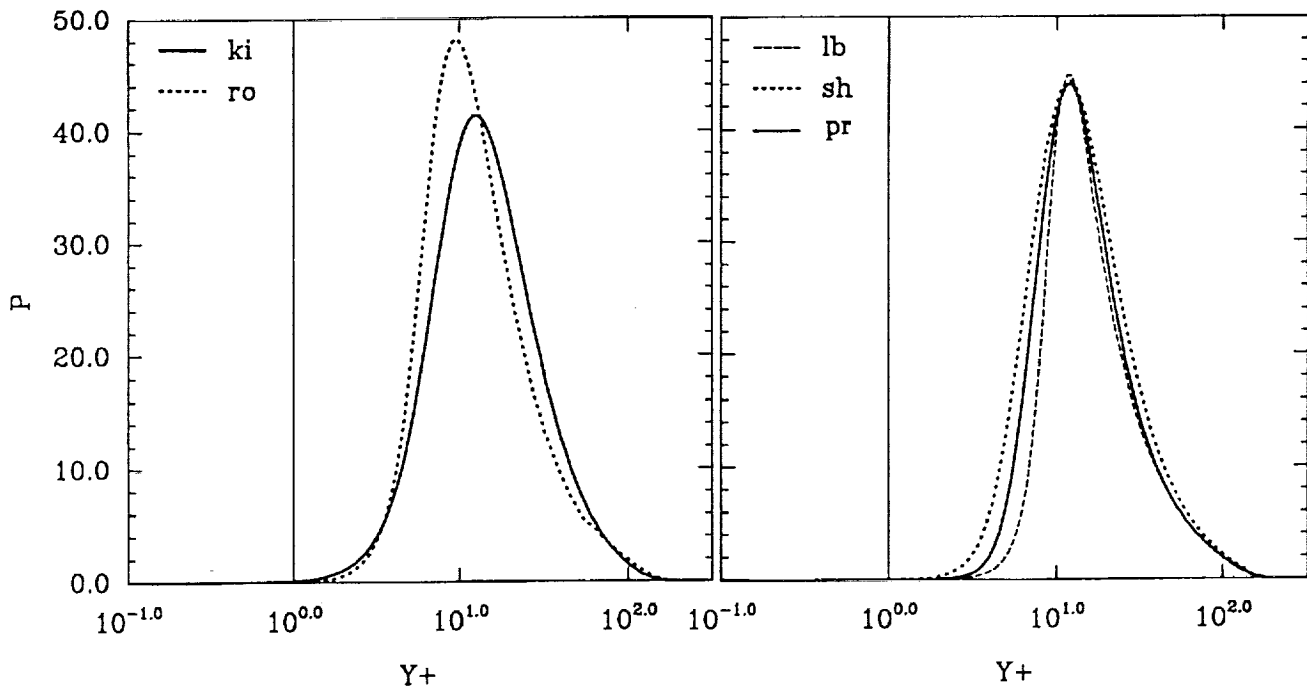
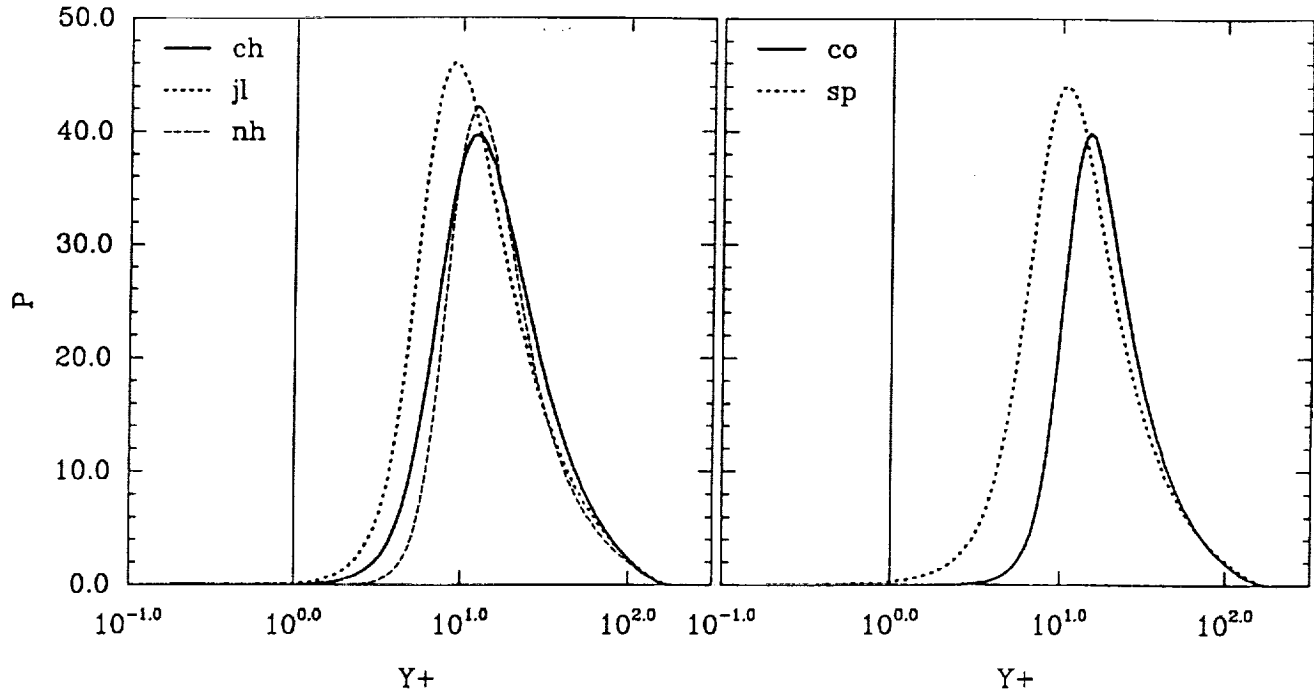


Figure 10: Production rate profiles

Report Documentation Page

1. Report No. NASA TM -104368 ICOMP-91-06; CMOTT-91-01		2. Government Accession No.		3. Recipient's Catalog No.	
4. Title and Subtitle Low Reynolds Number Two-Equation Modeling of Turbulent Flows				5. Report Date May 1991	
				6. Performing Organization Code	
7. Author(s) V. Michelassi and T.-H. Shih				8. Performing Organization Report No. E -6169	
				10. Work Unit No. 505-62-21	
9. Performing Organization Name and Address National Aeronautics and Space Administration Lewis Research Center Cleveland, Ohio 44135 - 3191				11. Contract or Grant No.	
				13. Type of Report and Period Covered Technical Memorandum	
12. Sponsoring Agency Name and Address National Aeronautics and Space Administration Washington, D.C. 20546 - 0001				14. Sponsoring Agency Code	
15. Supplementary Notes V. Michelassi and T.-H. Shih, Institute for Computational Mechanics in Propulsion and Center for Modeling of Turbulence and Transition, NASA Lewis Research Center (work funded under Space Act Agreement C-99066-G); V. Michelassi on leave from the University of Florence, Florence, Italy. Space Act Monitor: Louis A. Povinelli, (216) 433-4818.					
16. Abstract <p>A new $\kappa - \epsilon$ turbulence model that accounts for viscous and wall effects is presented. The proposed formulation does not contain the local wall distance thereby making very simple the application to complex geometries. The formulation is based on an existing $\kappa - \epsilon$ model that proved to fit very well with the results of direct numerical simulation. The new form is compared with nine different two-equation models and with direct numerical simulation for a fully developed channel flow at $Re = 3300$. The simple flow configuration allows a comparison free from numerical inaccuracies. The computed results prove that few of the considered forms exhibit a satisfactory agreement with the channel flow data. The new model shows an improvement with respect to the existing formulations.</p>					
17. Key Words (Suggested by Author(s)) Turbulence			18. Distribution Statement Unclassified - Unlimited Subject Category 34		
19. Security Classif. (of the report) Unclassified		20. Security Classif. (of this page) Unclassified		21. No. of pages 24	22. Price* A03

